Titanium Bioactive Surface Formation Via Alkali and Heat Treatments for Rapid Osseointegration

Marcelo Gabriel de Oliveira[a], Polyana Alves Radi[b] (ID) *, Danieli Aparecida Pereira Reis[b]* (ID) *,*

Adriano Gonçalves dos Reis[a]* (ID)

[a]Universidade Estadual Paulista (Unesp), Instituto de Ciência e Tecnologia, São José dos Campos, SP, Brasil.
[b]Universidade Federal de São Paulo, Programa de Pós-Graduação em Engenharia e Ciência de Materiais, São José dos Campos, SP, Brasil.

Titanium and its alloys are widely used as implant materials and many studies to accelerate the osseointegration have been performed. This work aims to evaluate the formation of a bioactive surface in commercially pure titanium (cp-Ti) grade 4 after alkali (AT) and heat treatments at 600 °C (AHT600) and 900 °C (AHT900). Characterization techniques were SEM, AFM, Raman, TF-XRD, wettability, nanoindentation and indentation adhesion. Additionally, SBF soaking tests were performed to evaluate apatite growth and showed that alkali and heat treatment accelerates apatite growth. The AT samples formed sodium hydrogen titanate (1 µm thick), and AHT600 and AHT900 formed sodium titanate (1 µm thick), while rutile TiO_2 increased with temperature, reaching up to 5 µm thick and the surface changed from slightly hydrophilic to fully hydrophilic. Roughness and surface area increased, especially in AHT900. The hardness of the surface layer was significantly increased by the heat treatment.

Keywords: Titanium, alkali-heat treatment, titanate.

1. Introduction

Commercially pure titanium (cp-Ti) and its alloys have been widely using as dental implant biomaterials due to its biocompatibility and good mechanical and corrosion resistance[1-5]. On the other hand, due to the bioinert properties of titanium, the bone formation rate (osseointegration) is very slow in the body[6]. Properties such as surface chemistry, texture, and wettability play a key role to accelerate the osseointegration of dental implants[7]. Hydrophilicity can alter bone cell adhesion, proliferation, and differentiation properties[8]. Increased surface roughness may induce strong bone-titanium interaction by increasing the bone-implant contact area[9]. In addition, the chemical characteristics of the altered surface can induce bone binding and affinity by promoting hydroxyapatite precipitation from body fluid[10,11].

In recent decades, several surface treatment studies have been conducted to improve osseointegration, such as plasma-spraying, sandblasting, and chemical treatments[12,13]. Among chemical treatments, alkali and heat treatment have been widely studied due to the simplicity of the method and ease of process control. Alkali and heat treatment consist of soaking the sample in a NaOH solution between 2 and 10 M and temperature between 60 and 100 °C for 24 hours to obtain a layer of sodium hydrogen titanate. Since this layer needs to be dehydrated and thickened, heat treatment is usually carried out between 600 and 800 °C to obtain a mechanically stable layer of sodium titanate. Previous studies have reported that Ti metal undergoing the alkali and heat treatment process has the potential to spontaneously form a bone apatite layer on its surface when soaked in SBF[14,15].

There are no studies in the literature reporting alkali and heat treatment at 900 °C with an in-depth evaluation of the structural changes occurring on the surface and cross-section of the material. In this context, the objective of this work is to evaluate the formation of a bioactive surface in cp-Ti grade 4 after alkali and heat treatment at 600 °C and 900 °C.

2. Materials and Methods

2.1. Alkali and heat treatments

A cp-Ti grade 4 ingot was machined into disks (12.7 mm in diameter and 3.0 mm thick) and used as substrate without treatment (WT). All samples were cleaned with acetone in an ultrasonic cleaner for a period of 20 min and dried at 40 °C. The samples used for alkali treatment (AT) were then soaked in an aqueous 5M NaOH solution at 60 °C under agitation for a period of 24 h. After being removed from the solution, these samples were gently rinsed with demineralized water and dried at 40 °C. Two groups of these alkali treated samples were subsequently heated to different conditions: 600 °C (AHT600) and 900 °C (AHT900), at a heating rate of 5 °C/min, kept at this temperature for an hour without atmosphere control and then let cool naturally in the furnace.

2.2. In vitro test

Treated (AT, AHT600, and AHT900) and untreated (WT) samples were soaked in 17 ml of SBF. The SBF preparation and sample soaking was performed according to Kokubo and Takadama[16]. The SBF ion concentration is nearly equal to those of human blood plasma at 36.5 °C (Table 1). After soaking in the SBF for 30 days at 36.5 °C, the samples were removed from the SBF, gently rinsed with demineralized water and dried at 40 °C.

2.3. Surface and cross-section characterization

The surface of the samples were examined by using a scanning electron microscope (SEM-FEG) Tescan Mira 3 with a coupled Energy Dispersive X-ray Spectroscopy (EDS, X-MAX - Oxford); optical profiler Veeco Wyko NT1100.

Atomic force microscope (AFM) model SPM 9500 J3 from Shimadzu; thin-film XRD (TF-XRD) by diffractometer Rigaku Ultima IV (Cu K α radiation, λ= 0.15405 nm) at 40 kV, 30 mA and a grazing incident angle of ω = 0.5° in the 2θ range of 20°–50°, Raman spectroscopy Horiba LabRam HR Evolution in the wavenumber of 100 to 1000 cm^{-1}.

The surface wettability was evaluated by contact angle measurements. The contact angles of the samples were assessed by dropping 10 μL of distilled water on specimens and measured using an image-based goniometer (Theta Lite Biolin Scientific).

Surface and cross-section hardness was measured by Nano Indentation Tester (NHT2) from Anton Paar with 10 mN of load during 10 seconds. The adherence of the formed layer was evaluated by using the VDI3198 indentation test[17] that enables the evaluation of the film's adhesion, cohesion, and brittleness. This test was performed using a Rockwell C diamond tip with a curvature radius of 200 μm and 150 kg load. This indentation corresponds to a contact pressure of around 18 GPa.

The cross-section of the samples was evaluated using a field emission scanning electron microscopy (FEG-SEM, MIRA3 - TESCAN) and a coupled Energy Dispersive X-ray Spectroscopy (EDS, X-MAX - Oxford) to analyze the elements and its distribution.

3. Results and Discussion

3.1. Surface Chemistry

Figure 1 shows the difference in the surface chemical composition of Ti before and after treatments, and it can be

Table 1. SBF Ion concentration.

Ion	Concentration (mM)
Na$^+$	142.0
K$^+$	5.0
Mg^{2+}	1.5
Ca^{2+}	2.5
Cl$^-$	147.8
HCO$_3^-$	4.2
HPO$_4^{2-}$	1.0
SO$_4^{2-}$	0.5

observed that the treatments altered the surface chemistry. The major surface compound changed from titanium (98% in WT) to oxygen (60%, 62%, and 68%, respectively for AT, AHT600, and AHT900). Moreover, in the treated samples the presence of approximately 3% sodium was observed.

These chemical changes on the surface are due to Ti reactions with NaOH. The mechanism of nanostructures formation in titanium can be considered a simultaneous process of dissolution and precipitation. At high NaOH concentrations, general titanium dissolution occurs and sodium titanate precipitation occurs. The general dissolution reaction of Ti in aqueous alkaline solution to form a titanate anion can be represented by[18]:

$$nTi + 2nH^+ + (2n+m)OH^- \rightarrow \left[Ti_nO_{2n+m}\right]^{(2m)-} + \left(\frac{4n+m}{2}\right)H_2 \qquad (1)$$
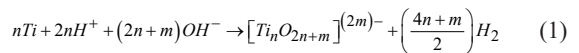
The titanate anions produced on dissolution may react with Na$^+$ cations in aqueous NaOH solution to produce sodium titanate. Equation 2 presents the general precipitation reaction of sodium titanate[18]:

$$2mNa^+ + \left[Ti_nO_{2n+m}\right]^{(2m)-} \rightarrow Na_{2m}Ti_nO_{2n+m} \qquad (2)$$
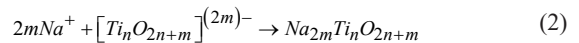
Sodium titanate formation was confirmed by TF-XRD and Raman analysis. Figure 2a shows the TF-XRD and Figure 2b shows the surface Raman profiles of Ti metal control and treated samples. From Figure 2 it can be seen that sodium hydrogen titanate (Na$_x$H$_{2-x}$Ti$_3$O$_7$) was formed on the metal surface by NaOH treatment (AT), and then was transformed into sodium titanate (Na$_2$Ti$_6$O$_{13}$), rutile and anatase by subsequent heat treatments (AHT600 and AHT900). In the AHT900 group, very sharp rutile phase peaks are observed, as a consequence of the treatment temperature (900 °C), increasing the reaction kinetics and oxygen diffusion on the titanium surface.

SEM images and EDX line profile of a cross-section of the surface layer of treated samples showed that the sodium and oxygen content gradually decreased, while Ti content increased near to a depth of 1 μm. It means that sodium hydrogen titanate (AT) and sodium titanate (AHT600 and AHT900) have around 1 μm depth.
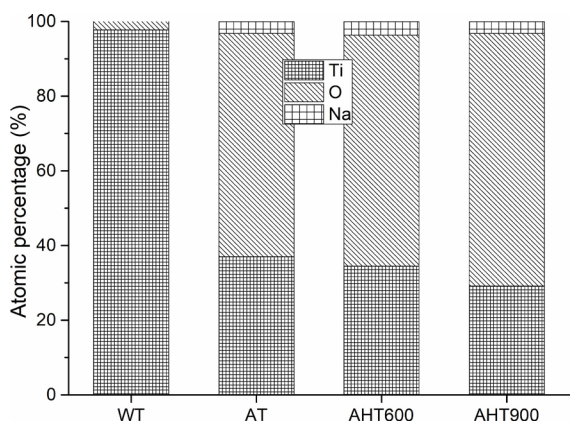

Figure 1. Weight percentages (wt%) of Ti, O, and Na as measured by energy-dispersive X-ray spectroscopy of the surface of WT, AT, AHT600, and AHT900.
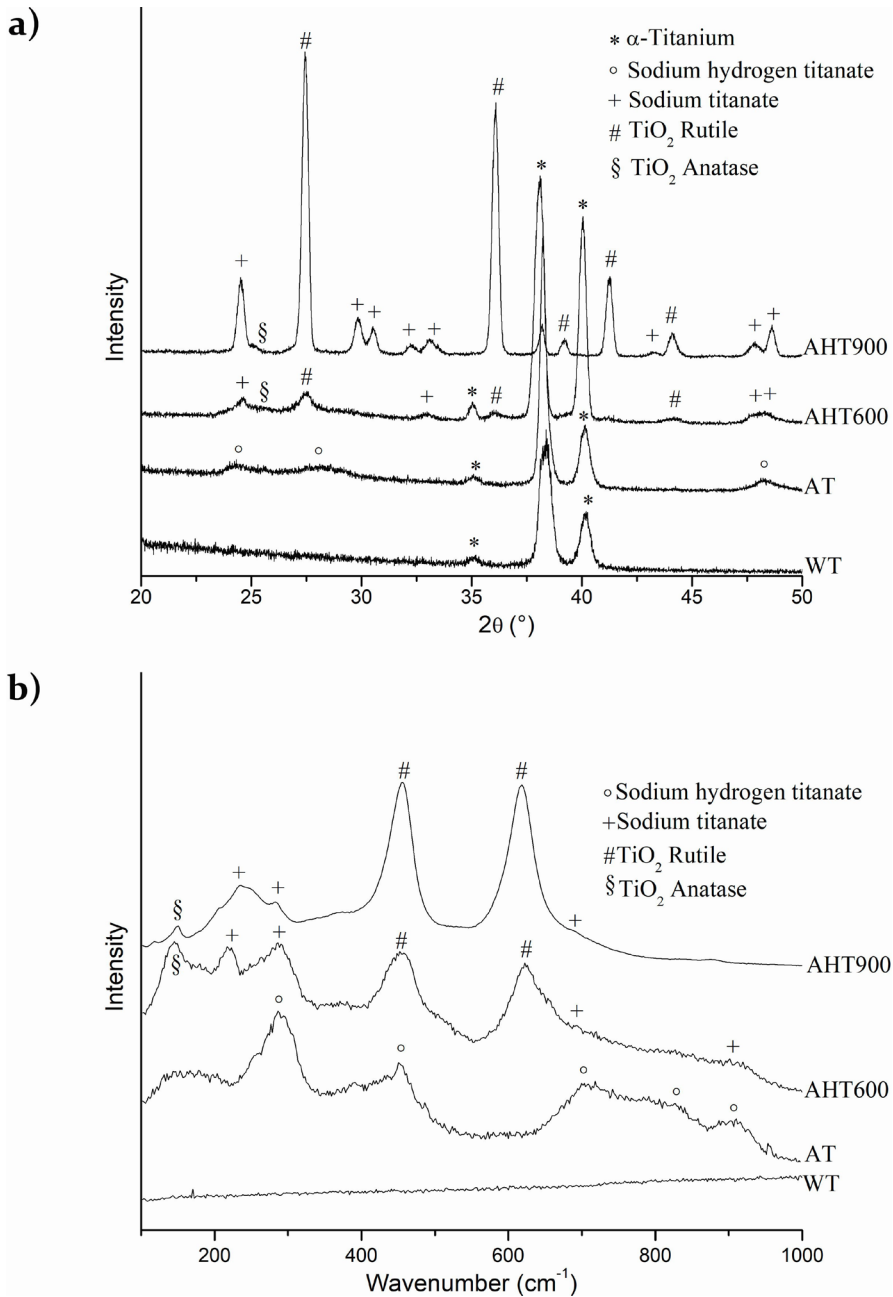
Figure 2. (a) TF-XRD and (b) Raman profiles of the surface of WT, AT, AHT600, and AHT900.

On the other hand, AHT900 showed a profile that oxygen content didn't decrease totally at 1 μm depth, but it was kept as high as Ti until around 6 μm when then finally the oxygen content was reduced and Ti was increasing according to the substrate. The greater depth of oxygen content for AHT900 is due to its greater oxygen diffusion, which is proportional to the applied temperature. Figure 3 shows an SEM image and EDX line profile of a cross-section of the surface layer of AHT900.

3.2. Surface topography and morphology

Figure 4 shows the changes in the surface topography of the Ti samples with respect to alkali and heat treatments.

The control sample (Figure 4a) showed machine marks and the treated samples showed peaks and valleys depending on variations in the treatment, being qualitatively more expressive in the AHT900 (Figure 4d). A quantitative analysis of the surface roughness was also performed based on the topographies of Figure 4. The average and standard deviations are shown in Figure 5. The quantitative analysis in Figure 5 corroborated with the qualitative analysis of Figure 4: According to Figure 5, there was a significant increase in total roughness on the microscale for AHT900 (32.3 ± 3.9 μm) compared to WT (7.0 ± 1.7 μm), AT (6.5 ± 1.7 μm), and AHT600 (6.6 ± 1.3 μm). A one-way ANOVA and Tukey analysis revealed a significant difference ($p < 0.05$) between

TQT900** and the other samples (WT*, AT*, and AHT600*), but without significant difference between WT*, AT*, and AHT600*. The literature also reported that the roughness didn't change, in similar conditions of treatment, when comparing WT with AHT600[19-21].
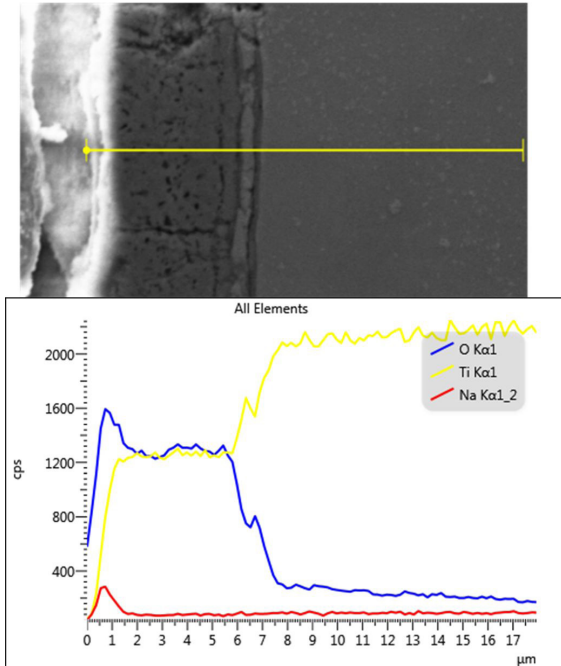

Figure 3. SEM image and EDX line profile of a cross section of the surface layer of AHT900.

Figure 6 shows the evolution of surface area after treatment. The same effect presented by roughness could be observed in the increase of surface area. The peaks and valleys generated due to increased roughness provided a larger surface area than a completely flat surface. From Figure 6 it can be observed that there was a significant increase in surface area for AHT900 ($299.3 \pm 48.4\%$) compared to WT ($5.3 \pm 1.2\%$), AT ($11.1 \pm 4, 2\%$), and AHT600 ($19.2 \pm 3.4\%$).

One-way ANOVA and Tukey analysis revealed a significant difference ($p < 0.05$) between the AHT900** and the other samples (WT*, AT*, and AHT600*). However, despite the trend of surface area growth presented in the results, the difference between the WT*, AT*, and AHT600* was not considered significant at a significance level of 0.05. By increasing the surface area it increases the area of contact between the metal and bone cells, improving the conditions for osseointegration[10,11].

FEG-SEM and AFM analyzes were performed and it can be seen in Figures 7 and 8, respectively. From Figures 7 and 8 it can be seen that the morphology of the formed surface is homogeneous and without the presence of microcracks. It is possible to observe that WT (Figures 7a and 8a) has a relatively flat surface with the presence of machining marks. From Figures 7b-d and 8b-d were observed in the formation of a finer, porous nanoscale structure that formed on the surface of Ti after alkali treatment (Figure 7b), and this microstructure basically did not change after heat treatment at 600 °C (Figure 7c). However, after heat treatment at 900 °C (Figure 7d), a distinct nanometric needle-like structure is observed, that is related to the TiO_2 rutile phase growing, resulting in an increased surface area and roughness reported in the Figures 5 and 6.
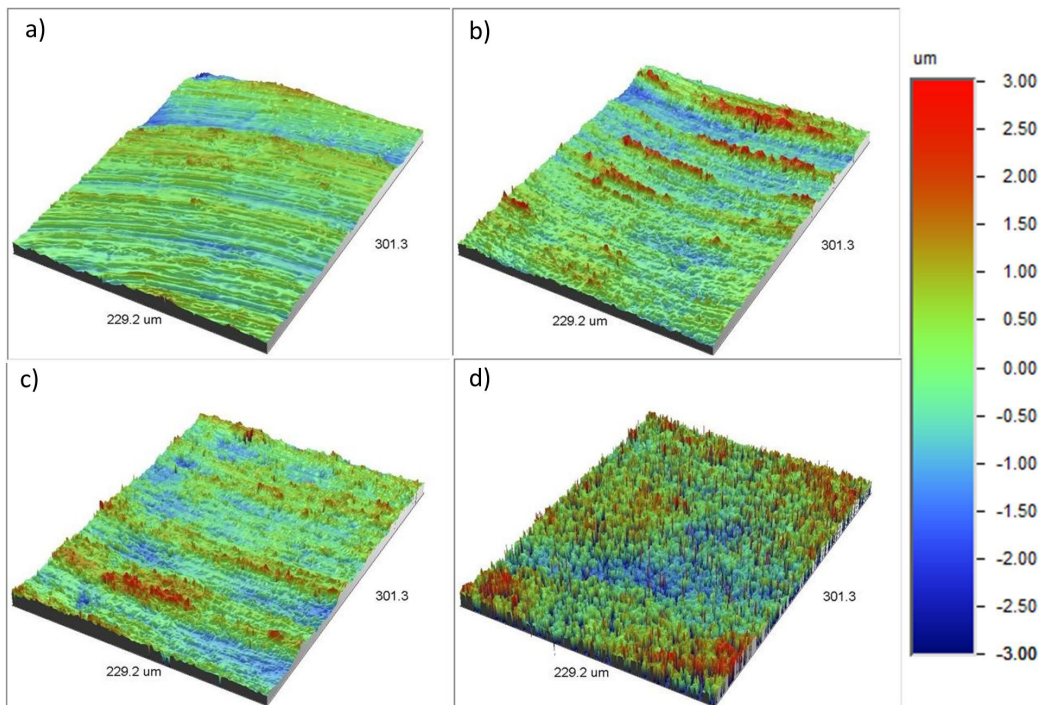

Figure 4. Profilometry topographies (area: 229.2×301.3 µm, scale: −3.0 to +3.0 µm) of machined Ti samples. (a) WT; (b) AT; (c) AHT600; and (d) AHT900.
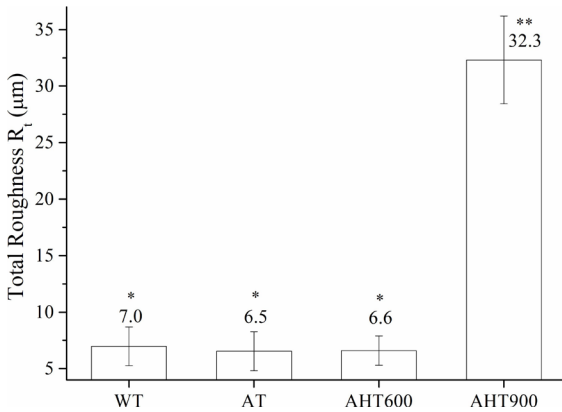
Figure 5. Ti Total roughness changes as a function of chemical and thermal treatment. * p < 0.05 compared to AHT900**.
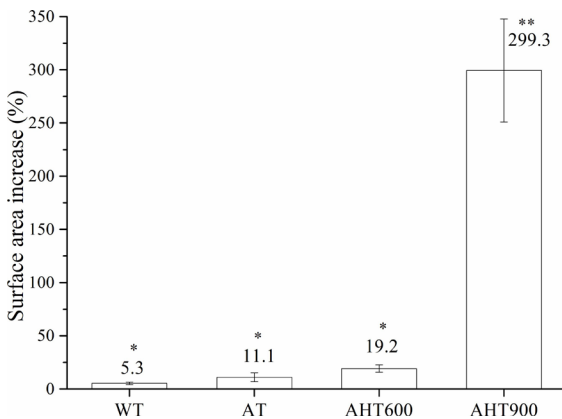

Figure 6. Ti surface area changes as a function of chemical and thermal treatment. * p < 0.05 compared to AHT900**.

3.3. Surface wettability

Figure 9 shows the contact angles of the samples before and after treatments, and the wettability of Ti was significantly changed from a partially hydrophilic surface in the WT group to a surface hydrophilic in the AT and AHT600 groups, and finally completely hydrophilic for the AHT900. Similar behavior is reported elsewere[19]. This change is probably due to the modification in texture (greater roughness and surface area) and chemical surface modification after alkali and heat treatments. By tailoring the functional groups available at the material surface, the surface wettability may also be altered. Hydrophilic surfaces can be constructed by the presence of polar functional groups. Sodium titanate is reported to have hydroxyl groups[22], a strong polar group, and it may have influenced the wettability enhancement. Surface wettability of a material is of vital importance for protein adsorption and cell adhesion. When an implant material is placed inside a human body, wetting of the implant material is among the first and most important events that occur by physiological fluids. This further controls protein adsorption, followed by cell attachment to the implant surface. Thus, surface wettability is considered an important criterion that may dictate implant osseointegration[23].

3.4. Surface and cross-section hardness

Figure 10 shows the surface hardness from treated and untreated samples. The surface hardness reduced from 483±74 HV (WT) to 276±66 HV (AT), and it is related to the porous surface created by the alkali treatment. A slight surface hardening recovery can be observed in the AHT600 sample (297±43 HV), but the surface hardening increase is more evident in the AHT900 (551±101 HV). The hardness increase is related to the TiO_2 rutile phase formation, according to XRD and Raman analysis (Figure 2).

Figure 11 shows the cross-section hardness profile. The analyses were made from 5 to 100 μm from the surface. AT sample did not change the hardness profile from the surface. AHT600 shows a higher hardness value (530 HV) at 5 μm, but after that, the results are similar to the substrate values. The higher hardness value at 5 μm in AHT600 is probably related to oxygen diffusion. AHT900 shows a hardness peak at around 15 μm (925 HV), and it's also related to oxygen diffusion that was more expressive when compared to AHT600, as shown by EDS profile from Figure 3. However, the substrate hardness of AHT900 (309 HV) was lower than AT (419 HV) and AHT600 (404HV). It is probably related to titanium annealing, reducing its hardness value.

3.5. Surface brittleness and cohesion

Figure 12 shows the indentation marks obtained on adhesion indentation test VDI3198 on (a) AT, (b) AHT600, and (c) AHT900. Both AT (Figure 12a) and AHT600 (Figure 12b) samples are classified as an acceptable failure due to and adequate interfacial adhesion. From Figure 12b (AHT600) is possible to observe some cracks around the indentation indicating a strong adherence but a brittle material, where the substrate piles up, but there is no indication of delamination. On the other hand, the AHT900 sample (Figure 12c) presented an unacceptable failure, where extended delamination at the vicinity of the imprint indicates poor interfacial adhesion, indicating a strongly adherent coating but also brittle one. The higher surface hardness from the AHT900 surface of 551 HV corroborates with this result.

3.6. In vitro test: apatite formation

Apatite formation was detected by SEM after being soaked in SBF for 30 days in the AT, AHT600, and AHT900 samples, but it was not detected in the WT sample. Figure 13 shows the SEM image of the surface of the AT sample, where it can be seen spherical particles that start to cover the entire surface. The apatite formation was more evident at the AT sample. Figure 14 shows the difference in surface chemical regarding Na, P, and Ca ions composition after being soaked in SBF for 30 days of WT, AT, AHT600, and AHT900 samples. Na, P, and Ca ions were chosen since it is an indication of apatite similar to bone mineral phase growing.

The WT sample didn't show Na^+ since it was not exposed to the alkali treatment. In addition to that, Ca and P ions were not detected in the WT sample, confirming that apatite didn't growth after 30 days of SBF soaking, corroborating with the SEM images. On the other hand, Na, P, and Ca ions were detected in the AT, AHT600, and AHT900 samples.

Ca and P ions were reduced with increasing temperature of heat treatment, and, at the same time, Na ions was increasing
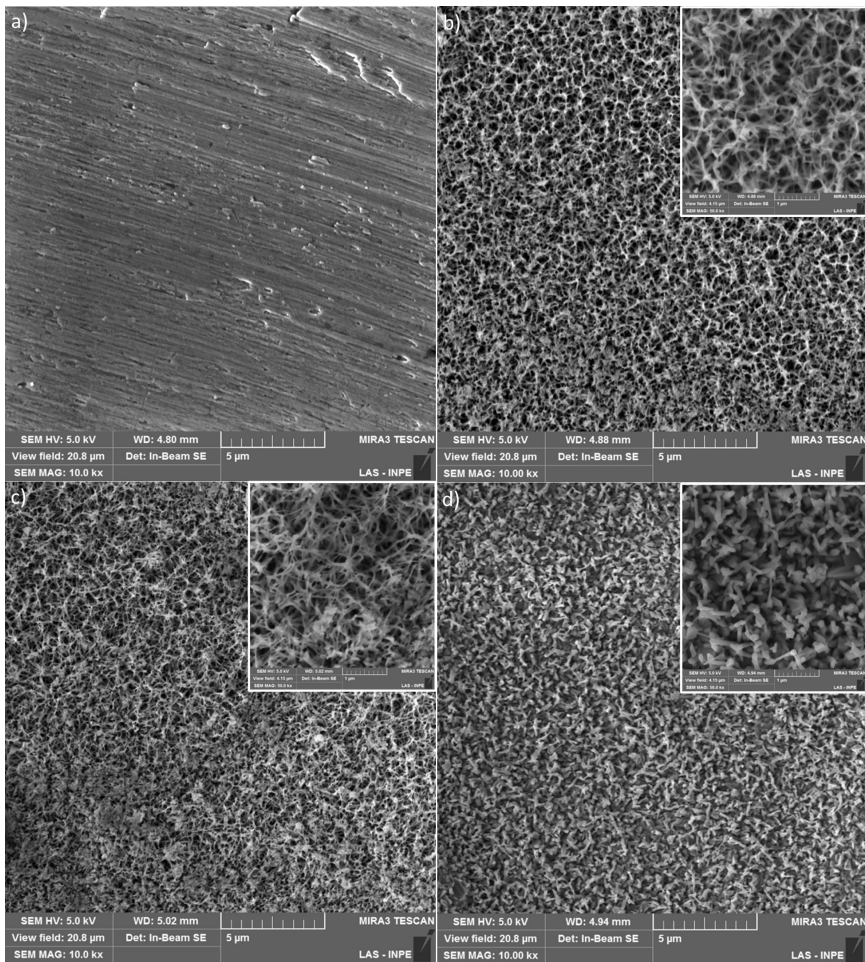
Figure 7. SEM images (10 kx) of Ti samples surfaces: (a) WT; (b) AT; (c) AHT600, and (d) AHT900. Insets show high-resolution images of nanotextures in 50 kx.
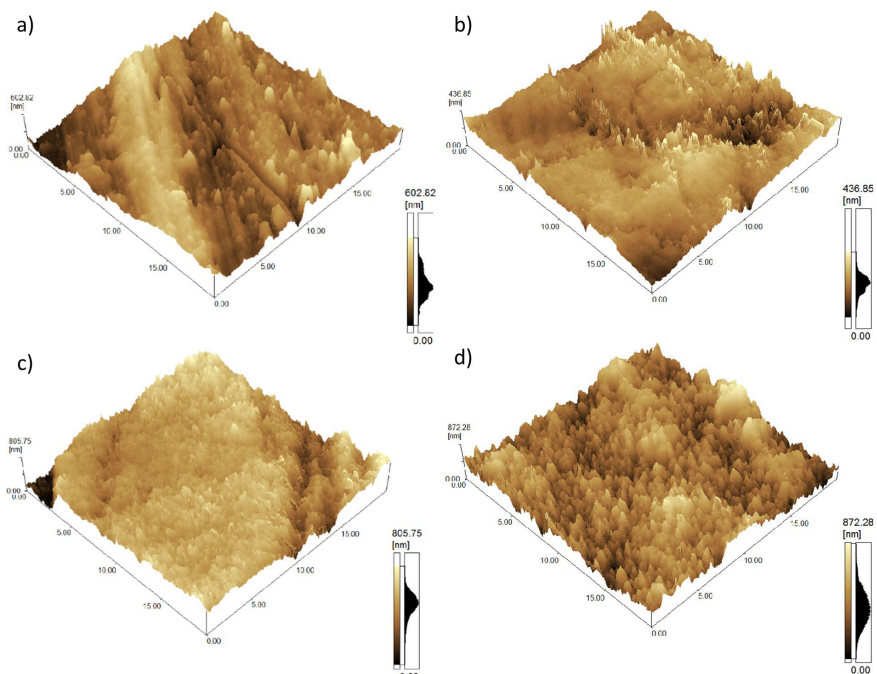

Figure 8. AFM topographies (area: 20 × 20 µm) of machined Ti samples. (a) WT; (b) AT; (c) AHT600; and (d) AHT900.

with the heat treatment. This is because during the immersion in SBF, Na ions release from sodium hydrogen titanate (AT) and from sodium titanate (AHT600 and AHT900) to react with a hydroxyl group (negatively charged) in the SBF.
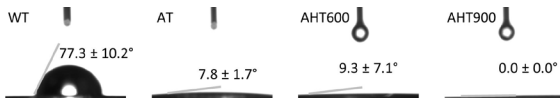

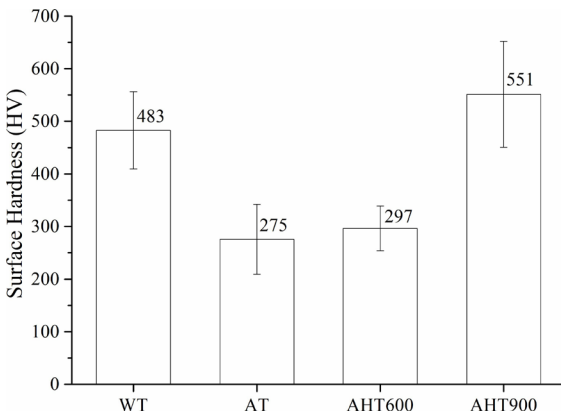**Figure 9.** Contact angles of Ti without treatment and surface-treated samples.

Figure 10. Surface hardness of WT, AT, AHT600, and AHT900.
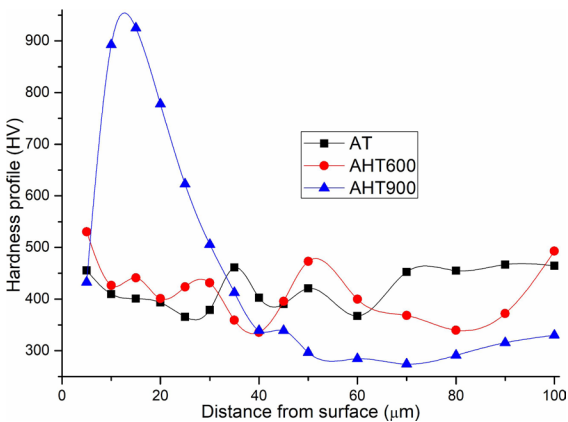

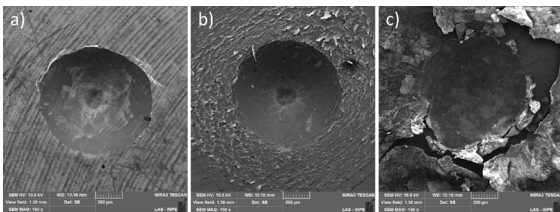**Figure 11.** Cross section hardness profile of WT, AT, AHT600, and AHT900.

Figure 12. FEG-SEM images showing the indentation mark performed on (a) AT, (b) AHT600, and (c) AHT900 samples, according to VDI 3198 [17].

Consequently, the surface attracts the positively charged Ca^+ ion which can be defined as a possible nucleation area for bone-like apatite formation. The calcium and phosphate ions are consumed since apatite nuclei are formed. The apatite growing on the substrates is directly affected by heat treatment.

The apatite rate formation decreases with heat treatment, especially at 900°C. It is associated with the Na ion release rate decrease from the densified sodium titanate after heat treatment (AHT600 and AHT900)[24-26].

Although AT samples forms a dense apatite after being soaked into SBF when compared with AHT600 and AHT900, sodium hydrogen titanate is too unstable for practical use. The more stable sodium titanate layer formed by the heat treatment is preferred (AHT600 and AHT900), from a practical point of view[27].

According to in vivo tests reported in the literature, titanium alkali and heat-treated surfaces bonds directly to the bone, but titanium surface that was only alkali-treated does not. The reason for that is the unstable reactive surface layer of alkali-treated titanium[28].
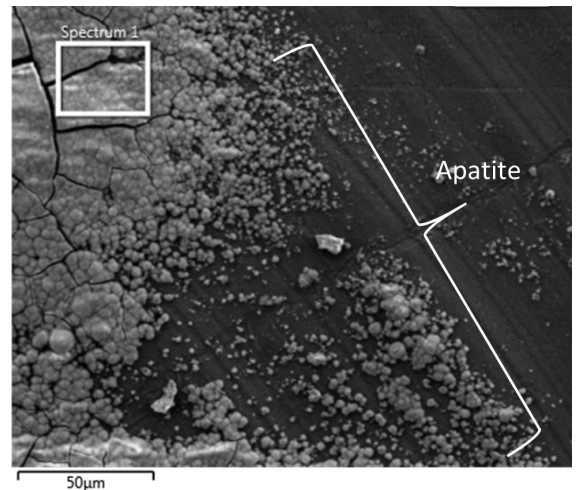

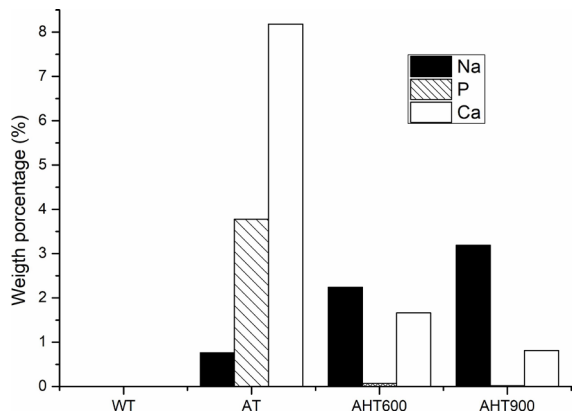**Figure 13.** The surface of AT soaked in SBF for 30 days.

Figure 14. EDX profiles of the surface after soaking in SBF for 30 days of WT, AT, AHT600, and AHT900.

4. Conclusions

Both alkali (AT) and alkaline heat treatment (AHT600 and AHT900) proved to be efficient to accelerate osseointegration due to the formation of sodium hydrogen titanate and sodium titanate, thus increased wettability, roughness, and surface area.

Alkali and heat treatments AHT600 and AHT900 showed to increase the mechanical resistance on the surface, but AHT900 showed high delamination after the indentation, besides reducing the mechanical resistance of the substrate due to annealing. The surface hardness and mechanical resistance of the top surface can be used to help define for which types of implants this superficial treatment is most suitable. Therefore, among the treatments tested, AHT600 proves to be the most suitable treatment to accelerate the osseointegration of cp-Ti grade 4.

The AHT900 demonstrated a huge increase in roughness, surface area and additionally are totally hydrophilic. Future in vivo experiments are recommended to compare AHT600 and AHT900 and evaluate the long-term osseointegration, in order to improve the results.

5. Acknowledgments

6. References

1. Shah FA, Trobos M, Thomsen P, Palmquist A. Commercially pure titanium (cp-Ti) versus titanium alloy (Ti6Al4V) materials as bone anchored implants: is one truly better than the other? Mater Sci Eng C. 2016;62:960-6.

2. Tini IRP, Araújo JCR, Gonçalves TF, Oliveira RM, Reis DAP, Reis AG, et al. Osteogenesis and biofilms formation on titanium surfaces submitted to oxygen plasma immersion ion implantation. Res Soc Dev. 2021;10(6):e37210615644.

3. Fabris V, Reginato VF, Smaniotto C, Bacchi A, Consani RLX. Treatment of resorbed mandibles with titanium plate and immediate implant-supported prosthesis: case series. Braz Dent J. 2019;30(3):244-51.

4. Sharma M, Soni M. Direct metal laser sintering of TI6Al4V alloy for patient-specific temporo mandibular joint prosthesis and implant. Mater Today Proc. 2021;38:333-9.

5. Kurup A, Dhatrak P, Khasnis N. Surface modification techniques of titanium and titanium alloys for biomedical dental applications: a review. Mater Today Proc. 2021;39:84-90.

6. Ankha MDVEA, Silva AM, Prado RF, Camalionte MP, Vasconcellos LMR, Radi PA, et al. Effect of DLC films with and without silver nanoparticles deposited on titanium alloy. Braz Dent J. 2019;30(6):607-16.

7. Santos ED, Luqueta G, Rajasekaran R, Santos TB, Doria ACOC, Radi PA, et al. Macrophages adhesion rate on Ti-6Al-4V substrates: polishing and DLC coating effects. Res Biomed Eng. 2016;32(2):144-52.

8. Toffoli A, Parisi L, Tatti R, Lorenzi A, Verucchi R, Manfredi E, et al. Thermal-induced hydrophilicity enhancement of titanium dental implant surfaces. J Oral Sci. 2020;62(2):217-21.

9. Swain S, Rautray TR. Effect of surface roughness on titanium medical implants. In: Thakur VK, editor. Materials horizons: from nature to nanomaterials. Singapure: Springer; 2021. p. 55-80.

10. Le Guéhennec L, Soueidan A, Layrolle P, Amouriq Y. Surface treatments of titanium dental implants for rapid osseointegration. Dent Mater. 2007;23(7):844-54.

11. Bagno A, Di Bello C. Surface treatments and roughness properties of Ti-based biomaterials. J Mater Sci Mater Med. 2004;15(9):935-49.

12. Shibata Y, Tanimoto Y. A review of improved fixation methods for dental implants. Part I: surface optimization for rapid osseointegration. J Prosthodont Res. 2015;59(1):20-33.

13. Alberti CJ, Saito E, Freitas FE, Reis DAP, Machado JPB, Reis AG. Effect of etching temperature on surface properties of Ti6Al4V alloy for use in biomedical applications. Mater Res. 2019;22(Suppl. 1):e20180782.

14. Yamaguchi S, Takadama H, Matsushita T, Nakamura T, Kokubo T. Cross-sectional analysis of the surface ceramic layer developed on Ti metal by NaOH-heat treatment and soaking in SBF. J Ceram Soc Jpn. 2009;117(1370):1126-30.

15. Li N, Xu W, Zhao J, Xiao G, Lu Y. The significant influence of ionic concentrations and immersion temperatures on deposition behaviors of hydroxyapatite on alkali- and heat-treated titanium in simulated body fluid. Thin Solid Films. 2018;646:163-72.

16. Kokubo T, Takadama H. How useful is SBF in predicting in vivo bone bioactivity? Biomaterials. 2006;27(15):2907-15.

17. Vidakis N, Antoniadis A, Bilalis N. The VDI 3198 indentation test evaluation of a reliable qualitative control for layered compounds. J Mater Process Technol. 2003;143–144(1):481-5.

18. Divya Rani VV, Manzoor K, Menon D, Selvamurugan N, Nair SV. The design of novel nanostructures on titanium by solution chemistry for an improved osteoblast response. Nanotechnology. 2009;20(19):195101.

19. Kamo M, Kyomoto M, Miyaji F. Time course of surface characteristics of alkali- and heat-treated titanium dental implants during vacuum storage. J Biomed Mater Res B Appl Biomater. 2017;105(6):1453-60.

20. Nishiguchi S, Fujibayashi S, Kim HM, Kokubo T, Nakamura T. Biology of alkali- and heat-treated titanium implants. J Biomed Mater Res A. 2003;67(1):26-35.

21. An S-H, Matsumoto T, Miyajima H, Sasaki J-I, Narayanan R, Kim K-H. Surface characterization of alkali- and heat-treated Ti with or without prior acid etching. Appl Surf Sci. 2012;258(10):4377-82.

22. Cruz AL, Ramos AP, Pazos LM, Parodi MB, Ybarra GO, Ruíz JEG. Effect of chemical and thermochemical treatments on the surface properties of commercially pure titanium. Materia. 2020;25(4):e-12846.

23. Paital SR, Dahotre NB. Calcium phosphate coatings for bio-implant applications: materials, performance factors, and methodologies. Mater Sci Eng Rep. 2009;66(1-3):1-70.

24. Butev E, Esen Z, Bor S. In vitro bioactivity investigation of alkali treated Ti6Al7Nb alloy foams. Appl Surf Sci. 2015;327:437-43.

25. Kim HM, Miyaji F, Kokubo T, Nishiguchi S, Nakamura T. Graded surface structure of bioactive titanium prepared by chemical treatment. J Biomed Mater Res. 1999;45(2):100-7.

26. Liang F, Zhou L, Wang K. Apatite formation on porous titanium by alkali and heat - treatment. Surf Coat Tech. 2003;165(2):133-9.

27. Camargo WA, Takemoto S, Hoekstra JW, Leeuwenburgh SCG, Jansen JA, van den Beucken JJJP, et al. Effect of surface alkali-based treatment of titanium implants on ability to promote in vitro mineralization and in vivo bone formation. Acta Biomater. 2017;57:511-23.

28. Nishiguchi S, Nakamura T, Kobayashi M, Kim H-M, Miyaji F, Kokubo T. The effect of heat treatment on bone-bonding ability of alkali-treated titanium. Biomaterials. 1999;20(5):491-500.